Structural Investigation of CH_3S Adsorbed on Au(111)

Mehmet. F. Danışman, Loredana Casalis[†], Gianangelo Bracco[‡], Giacinto Scoles[*]

Department of Chemistry, Princeton University, Princeton NJ 08544

danisman@princeton.edu

[*]To whom all correspondence should be addressed. E-mail: scoles@princeton.edu

[†]Permanent address: Sincrotrone Trieste, Trieste, Italy. E-mail: lcasalis@princeton.edu

[‡]Permanent address: INFM and Department of Physics, University of Genova, Italy. E-mail: bracco@fisica.unige.it

Although Self-Assembled Monolayers made of long chains of n-alkanethiols ($CH_3(CH_2)_{n-1}SH$) on Au(111) have been extensively studied in the past, the driving forces behind the appearance of the $(3x2\sqrt{3})$ super lattice observed at full coverage are still not completely understood. In order to focus on the role played by the sulfur head group minimizing the interactions between chains and to dispose of the question of possible X-ray induced damage, we have carried out a He atom diffraction study of the adsorption of the shortest (n=1) thiol radical, obtained by dissociative adsorption of $(CH_3S)_2$, on the Au(111) surface. Contrary to what is currently reported in the literature, domains of

hexagonal ($\sqrt{3}$ x $\sqrt{3}$)R30^{o} structure are observed to convert into well ordered (3x2$\sqrt{3}$) superstructure after annealing time of few hours. Observation of forbidden peaks by the (3x2$\sqrt{3}$) model proposed by Fenter et al. suggests a distortion of the symmetry of the unit cell. Observed chemisorption and physisorption energies were in good agreement with the literature.

Introduction

Self-assembled monolayers (SAMs) of thiol-functionalized molecules on gold have been studied extensively because of their role as model systems to better understand self-organization of matter in two dimensions [1,2]. Their numerous technological applications in corrosion inhibition [3], nano-fabrication of electronic devices [4], sensors [5] and non-linear optics [6] are another reason for the considerable attention that these systems have enjoyed during the last 10 years.

Among all SAMs alkanethiols [$CH_3(CH2)_{n-1}SH$] on Au(111) are one of the best studied systems. In early scanning probe microscopy studies on alkanethiols Porter et al. observed a hexagonal ($\sqrt{3}$ x $\sqrt{3}$)R30^o lattice structure for chains with n=2,4-17 using both atomic force microscopy (AFM) [7] and scanning tunneling microscopy (STM) [8]. Using low energy electron diffraction (LEED), Dubois et al. [9] observed the same structure for n<3 whereas for 4<n<12 they reported larger unit cells (($m\sqrt{3}$ x $\sqrt{3}$)R30^o where m is an integer between 4 and 6 depending on the chain length). Both of the above mentioned groups assigned the threefold hollow site as the preferred adsorption site. In addition to the ($\sqrt{3}$ x $\sqrt{3}$)R30^o hexagonal lattice, a (3x2$\sqrt{3}$) super lattice was also observed by means of X-ray diffraction (XRD) [10,11], low energy atom diffraction (LEAD) [12-14] and STM techniques [15,16] for alkanethiols with n>8. Fenter et al. [10] attributed the origin of the superstructure to head group substrate interactions, and proposed a unit cell with two pairs of non equivalent sulfur atoms, each pair having one atom on the threefold hollow site and one on the bridge site, at relatively short distance from each other. The same group addressed the effect of chain length on 2-D packing structure for chains of n between 10 and 30 [11]. Although they observed two different

regimes for n<14 and n>16, distinguished by the tilt angle of the chains, caused by the balance between the interchain and substrate-headgroup interactions, they observed the (3x2√3) superstructure for all the alkanethiols measured in their studies.

In other studies, concentrated on shorter chain (n<6) and employing microscopy techniques several striped phases have been reported. Dishner et al. [17] reported in addition to a (3x2√3) structure a (2√3 x √3)R30^o striped phase for methanethiol SAMs. Voets et al. [18] reported striped phases for n=4-6 with unit cells (p x √3) (p=3 for n=4,5 and p=4 for n=6) on Au(111).

Recently several groups have investigated alkanethiol head-group substrate interaction from a theoretical point of view. In these studies, which employ density functional theory (DFT) methods, contradictory results are reported for the adsorption site of methanethiol on Au(111) surface. Yourdshahyan et al. [19] and Gronbeck et al. [20] indicate the fcc threefold hollow site as the most stable one, however Hayashi et al. [21] and Vargas et al. [22] found the bridge site as the most stable adsorption site. Vargas et al. were also able to identify a (3x2√3) super lattice with the sulfur atoms sitting on two different bridge sites, which was energetically indistinguishable from (√3 x √3)R30^o hexagonal lattice at full coverage. The behavior of dimethyldisulfide on Au(111) layer is also investigated by the above mentioned groups. The common result of all these studies was the dissociative adsorption of dimethyldisulfide on the Au(111) surface. The dissociative adsorption of dimethyldisulfide on Au(111) at room temperature has been also reported in several experimental studies where TPD [23], AFM [24], XPS [23,25], and STM [26] techniques have been employed. Although there are still some controversial results in the literature regarding to this issue, it is generally observed that the structures obtained

adsorbing either symmetric dialkyldisulfides or alkanethiols are indistinguishable from each other [2 and references there in].

Unfortunately the inconsistency between both experimental and theoretical studies results in an incomplete picture for the short chain alkanethiols. To contribute to a better understanding of this subject we have studied the structure of methanethiol on Au(111) obtained by dissociative adsorption of dimethyldisulfide (DMDS) by LEAD. Our results clearly indicate the presence of a $(3x2\sqrt{3})$ superstructure at saturation coverage. In absence of quantitative intensity calculations (presently in progress) we cannot at this time reach any conclusion on the nature of the binding site. Intensity calculations for He beam diffraction in such a highly corrugated system, with peak-to-valley corrugations of the order of one Ångstrom, have been so far unfeasible due to convergency problems in the solutions of the close-coupled multichannel scattering problem. As new, faster, programs have recently become available [27] these type of calculations are expected to deliver height information for the CH_3 groups and therefore to lead to insight also for the position of the Sulfur atoms.

Experimental

Here we will focus on the main characteristics of the He atom diffraction apparatus used in our experiments. For a more detailed description the reader is referred to previous publications [28,29]. A mono energetic helium beam was produced by supersonic expansion from a source, which was kept at 70 K. The energy of the He is about 14 meV with a dispersion of ~2%. The beam was collided with the surface at a constant incidence angle of $60^o \pm 0.5^o$, and the resulting diffraction pattern was detected by rotating a liquid

helium cooled bolometer (kept at 1.6 K by pumping on the liquid helium) around the surface in a horizontal plane containing the incident beam and the normal to the surface. The angular distribution of the scattered atoms was transformed to the momentum space by using the equation:

$$\Delta K_{//} = k_i (\sin \theta_f - \sin \theta_i)$$

where $\Delta K_{//}$ is the parallel momentum transfer, k_i and θ_i are the incident wave vector and angle, and θ_f indicates the angular position of the detector. Since there is widespread agreement on the fact that the CH_3S over layer is commensurate with the Au(111) mesh, the incident wave vector, k_i, was calibrated using the (-1,0) and (-2,0) hexagonal diffraction peaks of the methanethiol layer and calculated to be 5.1 $Å^{-1}$ at the source temperature of 70 K. The diffraction geometry is shown in fig. 1a, where K_f - K_i represents parallel momentum transfer $\Delta K_{//}$.

The detector, the crystal and the doser were housed in two concentric radiation shields cooled by Liquid Nitrogen (fig. 1b). This shield in conjunction with the cryopumping action of the liquid helium 1.6 K cryostat provides for extremely (actually, immeasurably) low pressures for all gasses but H_2 and He in the scattering environment. The crystal manipulator has three degrees of freedom for the crystal and one for the detector, which correspond to the polar (θ_i), azimuthal (ϕ) and tilt (χ) angle of the crystal and the polar rotation of the detector (θ_f). θ_i determines the Helium beam incidence angle and was kept constant during the course of this study. The high sensitivity of bolometer detector at low crystal temperatures (the minimum detectable flux is ~$5x10^8$

atoms/second at 70 K primary beam source temperature) enables a very efficient detection of diffracted helium as the primary beam flux of ~ $4x10^{14}$ He atoms/second can be detected with a S/N ratio of 5000. However at elevated sample temperatures two effects cause a reduction of the detected intensity. The first is due to attenuation of the Helium elastic diffraction signal caused by thermal-motion of the surface atoms (Debye-Waller effect). The second is due to the radiation emanating from the crystal which heats the bolometer shifting its working point and substantially reducing its sensitivity. Although specular reflection can still be detected up to 550 K (crystal substrate temperature), diffraction patterns cannot be observed above 150 K. For this reason all diffraction measurements were performed at 40 K crystal temperature.

The Au(111) surface was cleaned under ultra high vacuum through several sputter-anneal cycles (15-30 minutes) with Ar pressure of 1.3-1.5$x10^{-5}$ torr and Ar^{+} energy of 1.0 keV. The cleanliness of the surface was verified by the observation of the (0,-1) diffraction and (23 x $\sqrt{3}$) reconstruction peaks of Au(111). Self-assembled monolayers of dimethyldisulfide were prepared by deposition from the gas phase through the doser shown in fig. 1b. Dimethyldisulfide was purified by several freeze-pump-thaw cycles prior to deposition. The molecular flux, *f*, on the crystal surface was determined from the 1/e decay time, τ, of the specular signal (the sticking coefficient was assumed to be unity) by the use of equation

$$f = (\Sigma\tau)^{-1}$$

where Σ is the effective cross section of dimethyldisulfide [29] which was assumed to be ~165 $Å^2$.

Results and Discussion

Diffraction scans, taken along the <1-10> direction ($\phi=0^o$) after different DMDS dosing and annealing procedures, are shown in fig. 2a. Curve 1 was obtained after exposing the gold surface kept at 200 K to a flux of ~5 x 10^{13} molecules.$cm^{-2}s^{-1}$, which corresponds to 0.33 Langmuirs/s for 100 seconds followed by annealing at 330 K for 100. The ($\sqrt{3}$ x $\sqrt{3}$) hexagonal peaks at 1.45 $Å^{-1}$, 2.90 $Å^{-1}$ and 4.36 $Å^{-1}$ are clearly visible in this curve (hereafter referred as structure 1). In addition, few more peaks can be identified around the first and third order hexagonal peaks, which are indications of a larger unit cell. However, these peaks are not well resolved because of the small domain sizes. To ensure complete surface coverage, after the annealing a second dosing was performed. During this second dosing process the surface temperature was ramped from 200 K to 275 K for a total deposition period of ~7 minutes. After dosing, the sample was annealed at 320 K for ten minutes and the second curve of fig. 2a (structure 2) was obtained. Although the larger unit cell peaks were resolved well it was still impossible to determine the peak positions precisely enough for a structure determination. In order to increase further the domain size, the film was kept at 290 K over night. A diffraction scan taken after this period is shown in the third curve of fig. 2a (structure 3) where the larger unit cell peaks were well separated from the hexagonal peaks. To further investigate the evolution of the system as a function of annealing time and temperature we annealed the surface at 330 K for 15 minutes. As can be seen from the fourth curve in fig. 2a this annealing process led

to a structure, which was identical to the first one. We then tried to optimize the deposition temperature and annealing temperature to get better resolution. The best results (well resolved structure 3) were obtained by the procedure detailed above. We were not able to get structure 3 by deposition of DMDS on the clean Au(111) surface without going through structure 1.

The diffraction characteristics of the above mentioned three structures are summarized in fig. 2b. The higher specular intensity and peak width of structure 1 suggest that this phase is composed of small islands that do not cover the Au(111) surface entirely. We believe that the DMDS molecules deposited at 200 K stick where they land and cannot diffuse on the surface because of their low mobility at this temperature. This results in a random distribution of the molecules on the surface with a low packing density, which, before annealing, reduces the chance of incoming DMDS molecules to find a free adsorption site and cause saturation. The packing density of the (3x2$\sqrt{3}$) phase is 4.6 x 10^{14} thiolate molecules/cm^2. If the DMDS molecules are approximated as spheres with a radius of 4.6 Å (which is half the van der Waals length of DMDS molecule in trans configuration) and are assumed to pack in a hexagonal lattice with a lattice constant of 9.2 Å, a packing density of 2.7 x 10^{14} thiolate molecules/cm^2 can be obtained. This suggests that adsorption at 200 K results in a surface coverage that is not more than 60% of that of the (3x2$\sqrt{3}$) phase. Upon annealing to 330 K molecules rearrange and form domains of the (3x2$\sqrt{3}$) superstructure leaving a fraction of the Au(111) surface uncovered, which results in higher specular reflection. To predict the specular intensity as a function of surface coverage, the maximum attraction model proposed by Poelsema and

Comsa [30] can be applied. According to this model the specular intensity is given by the following equations

$I/I_0 = 1 - n_s.U.\Theta$ for islands larger than the transfer width

$I/I_0 = (1 - n_s.U.\Theta)^2$ for islands smaller than the transfer width

where I_0 is specular intensity at zero coverage, n_s is the packing density of the substrate atoms, U is the unit cell size of the adsorbate and Θ is the coverage. If the coverage for curve 3 is assumed to be 0.9 ML (we define 1 ML as the adsorbate density which is equal to 1/3 of that of gold atoms) and that of curve 1 to be 0.54 ML (60% percent of 0.9) a specular intensity ratio of 0.49 can be obtained by using the above-mentioned equations. This value is in good agreement with the experimental intensity ratio of curve 3 to curve 1 which is ~0.5.

The average domain size depends on the migration to the steps of the so-called "etch pits" [15], which is a slow process and involves rearrangement of the position of atoms of the substrate. This rearrangement of the substrate occurs rapidly only at temperatures at which this short chain thiol may start evaporating. The annealing procedure may also introduce in the system some disorder and result in lower density structures in addition to the $(3x2\sqrt{3})$ domains. Lower density striped structures made of missing rows of methanethiol either on Au (111) nearest neighbor or the next nearest neighbor direction have been observed by Dishner et al. [17]. However the broad feature of the diffraction pattern of structure 1 and the coincidence of the peak positions of these striped phases with that of $(3x2\sqrt{3})$ super lattice makes it impossible for us to draw a certain conclusion

about the arrangement of the organic over layer. We believe that this relatively low coverage phase (structure 1) acts as a nucleation center and upon further deposition the (3x2√3) phase grows from the pre-existing islands. Increasing the dosing results in a higher packing density and the transformation of any existing striped phase to the denser (3x2√3) structure. Upon further annealing, the sample increases the domain size, which results in structure 3. The transformation of structure 3 back to structure 1 is caused by the desorption of the organic species during the annealing procedure at 330 K. If the annealing period is lengthened, the specularity of structure 1 increases and new broad peaks near the specular appear which we think is an indication of the increasing striped phase coverage. This fact is clearly visible in fig. 3 where the change in diffraction pattern of structure 1 as a function of annealing temperature and period is shown. In previous LEAD [12,31] and LEED [32] studies on decanethiol it was observed that high quality samples kept their high density (3x2√3) rectangular form up to 350-370 K. Annealing the samples to higher temperatures resulted in several striped phases named as (px√3) where p indicates the distance between the stripes in units of Au(111) nearest neighbor distance. With increasing annealing temperature, the separation between the stripes increases and the (3x2√3) phase disappears completely. The decrease in coverage was attributed to the desorption of the thiolate molecules during the annealing process. When the difference between the interchain interactions of longer and shorter chain alkanethiols is taken into account, it is reasonable to observe such phase transitions, from a high density (3x2√3) phase to a lower density structure, at lower temperatures for methanethiol.

We also recorded specular reflection data as a function of crystal temperature for determining desorption energies of the organic monolayers. The raw specular intensity data for structure 1 and structure 3 are shown in fig. 4a. It should be noted that these curves result from the change in surface coverage and the thermal motion of the surface molecules, so they are not a direct measure of desorbed species. However peak desorption temperatures that are needed to estimate desorption energies can still be determined after a differentiation of raw intensity data. The "traditional TPD" curves, which result after differentiating the raw data (corrected for bolometer sensitivity changes and Debye-Waller attenuation) are also shown in fig. 4b. For these corrections the temperature dependence of the specular reflection signal of the clean Au(111) surface was used (fig. 4a). Peak desorption temperatures were 432 ± 2 K and 437 ± 2 K for structure 1 and structure 3 respectively. The corresponding desorption energy value determined after a Redhead analysis [33] assuming a first order desorption and using a pre-exponential factor of 10^{13} s^{-1} is 117 ± 3 kJ/mol. This value is, very close to the previously reported chemisorption energies for alkanethiols (126 ± 2 kJ/mol) [34]. The difference may be caused by the systematic errors.

The temperature dependence of the specular intensity, before desorption starts is a measure of the stiffness of organic over-layer. Since the thermal motion of more rigid lattices will increase less rapidly with temperature than that of softer lattices, thermal attenuation of the specular intensity will be slower for rigid lattices. When the specular intensity variation of structure 3 with temperature was compared with that of structure 1 a slower decay could be observed. This observation leads to the conclusion that structure 3 is more rigid than structure 1, which is another support for the higher packing density of

former structure. We exclude at this point the presence of physisorbed species either at the bare Au or on top of the (3x2$\sqrt{3}$) domains. In a separate experiment in fact we deposited DMDS at 200 K on top of structure 1, and we observed a desorption peak at 237 ± 3 K. This temperature gives a desorption energy of 62 ± 2 kJ/mol which is in good agreement with the bond additive model proposed by Wetterer et al. (69.8 ± 3.5 kJ/mol) [35] for the physisorption of hydrocarbons on Au(111). Since both structure 1 and structure 3 were measured after annealing to ~300 K, they should involve only chemisorbed molecules.

For determining the unit cell of structure 3 we mapped the reciprocal space of this structure by taking diffraction scans at azimuthal angles, ϕ, between -30^o and 30^o (with respect to the gold nearest-neighbor direction <1-10> which is set to $\phi=0^o$) with 5^o increments. Some representative scans are shown in fig. 5. For a better understanding of these curves we should note, at this point, the structure of our detector, which is designed to optimize the polar angle (θ) resolution, whereas the resolution in azimuthal angle (ϕ) is proportional to $\Delta K_{//}$ and can be as low as 40^o for $\Delta K_{//}$ = 0.5 $Å^{-1}$ (A more detailed discussion of this subject can be found in ref. 28 and 29). For this reason at any given azimuth off azimuth peaks are also detected especially for small $\Delta K_{//}$ values. This is clearly visible in fig. 5, where peaks between 0.6 $Å^{-1}$ and 2.0 $Å^{-1}$, which belong to different azimuthal angles, appear in all of the spectra.

To identify the peak centers precisely diffraction scan curves are fitted to Lorentzians after a cosine background subtraction. A polar plot of peak positions versus azimuthal angle, ϕ, (K_x vs K_y) determined in this way is shown in fig. 6. On the same graph the reciprocal space lattice for the (3x2$\sqrt{3}$) and the ($\sqrt{3}$ x $\sqrt{3}$)R30^o hexagonal lattice are also

shown. The (3x2√3) reciprocal space pattern shown in this graph is a result of three equivalent (3x2√3) domains rotated 120^{o} with respect to each other. For the sake of clarity real space and reciprocal space illustration of these domains are shown in fig. 7. It can be seen in fig. 6 that the diffracted peak positions fit quite well with the (3x2√3) lattice points within the experimental limits. Most of the experimental points can be assigned to either an "on" or an "off" azimuth peak of the (3x2√3) mesh. We compared several striped and centered unit cell structures with the experimental points but none of these structures produced a better fit than the (3x2√3) phase.

Although the comparison in fig. 6 gives a qualitative idea about the structure, for a better description the peak intensities should also be considered. For this purpose the intensity ratios of the (0,-1)'' peak to (-1,0)' peak and (0,-2)'' peak to (-2,0)' peak of the (3x2√3) lattice are plotted in fig. 8, with changing azimuthal angle. It can clearly be seen in this plot that the (-1,0)' and (-2,0)'peaks are more intense for ϕ=0^{o} and (0,-1)'' and (0,-2)'' peaks are more intense at ϕ=30^{o}, which is consistent with a (3x2√3) unit cell. However for the (3x2√3) unit cell proposed by Fenter et al. [9] for longer chain alkanethiols, the (-1,0) and (0,-2) peaks should not be observed because of symmetry restrictions: according to this model in fact molecules 1 and 2 in fig. 6a are identical as well as molecules 3 and 4. For these peaks to be observed all the thiolate molecules in the unit cell (molecules 1,2,3 and 4 in fig. 7a) should be non-equivalent. This observation also lets us to discard the possibility of formation of a striped (3x2√3) phase as reported by Dishner et al. Since in their case molecules 1 and 2 were identical and molecules 3 and 4 were missing.

Deviations from the proposed (3x2√3) structure were also reported by Camillone et al. for decanethiol (n=10) on Au(111). But in their study, the observed intensities for these forbidden peaks were very small when compared with the (-2,0)' and (0,-1)'' peaks which was interpreted as a small distortion of the originally highly symmetric structure. However in our case intensities of these peaks are comparable with the (-2,0)' and (0,-1)'' peaks (fig. 8), which indicates a higher distortion of symmetry. In fig. 9 the (3x2√3) unit cell proposed by Vargas et al. for methanethiol on Au(111) is shown. In this structure methanethiol molecules occupy two different bridge sites, and they have the same symmetry with the unit cell proposed by Fenter et al.[9], which does not agree with our observations. However we should note that in this calculations dispersion forces between the carbon groups are not taken into account. It is possible that when these forces are also considered molecules 2 and 4 may deviate from their original positions in order to reduce the repulsive interaction. Such a distortion may lead to the observation of the originally forbidden peaks.

Conclusions

We have performed a study of the structural evolution of methanethiol on Au(111) surface by Helium atom diffraction. Although we believe that at lower surface coverage the overlayer consists of small domains of (3x2√3) structure we can not discard the possibility of existence of striped phases. Further dosing enhances surface coverage and, upon annealing at 290 K, a well-ordered (3x2√3) phase can be obtained. Formation of the complete (3x2√3) phase in a stepwise manner can be explained by the fact that, without annealing, it is not possible to achieve saturation coverage. Conversely, we found

that annealing the sample at still higher temperatures (330 K) results in the transformation of the high density (3x2√3) phase to a lower coverage phase that (like structure 1) may be a mixture of (3x2√3) and striped islands. This desorption temperature is reasonable in view of the fact that methanethiol has smaller interchain interactions than the larger thiols [36]. These results reveal that formation of (3x2√3) phase is a matter of sample preparation. Provided the right deposition conditions and annealing period for system to reach the equilibrium there is no reason to not to obtain (3x2√3) super lattice, regardless of the chain length of the thiolate species. In view of the disagreement with theoretical predictions [22] it becomes necessary to have a second look at the hypotheses that are at the basis of the theoretical model.

Observed chemisorption and physisorption energies were in good agreement with the literature. Observation of the peaks forbidden by the symmetry of the previous models indicates a larger distortion in the symmetry of the unit cell. The large number of diffraction channels caused by large surface corrugation of the (3x2√3) phase hinders a simple quantitative analysis of the diffraction pattern. To account for the distortion of the unit cell and the surface corrugation we are currently working on quasi exact quantum mechanical calculation of the He diffraction intensities from a methanethiol layer on Au(111) in collaboration with the group of D. Farias of the Autonomas University of Madrid and hope to address this problem again in a future publication.

Acknowledgement

This work was supported by DOE Materials Division under contract DE-FG02-93ER45503. M.F.D. thanks Higher Education Board of Turkey for financial support.

References

[1] Ulman, A. Chem. Rev. **1996**, 96, 1533.

[2] Schreiber, F., Prog. Sur. Sci. **2000**, 65, 151.

[3] Scherer, J.; Vogt, M. R.; Magnussen, O. M.; Behm, R. J. Langmuir **1997**, 13, 7045.

[4] Schon, J.H.; Meng, H.; Bao, Z.; Nature **2001**, 413, 713.

[5] Ulman, A. An Introduction to Ultra-thin Organic Films, Acedemic Press : New York, 1991.

[6] Swallen, J. D.; Allara, D. L.; Andrade, J. D.; Chandross, E. A.; Garoff, S.; Israelachvili, J.; McCarthy, T. J.; Murray, R.; Pease, R. F.; Rabolt, J. F. ;Wynne, K. J.; Yu, H. Langmuir **1987**, 3, 932.

[7] Alves, C. A.; Smith, E. L.; Porter, M. D. J. Am. Chem. Soc. **1992**, 114, 1222.

[8] Widrig, C. A.; Alves, C. A.; Porter, M. D. J. Am. Chem. Soc. **1991**, 113, 2805.

[9] Dubois, L. H.; Zegarski, B. R.; Nuzzo, R.G. J. Chem. Phys,**1993**, 98, 678.

[10] Fenter, P.; Eberhardt, A.; Eisenberger, P. Science,**1994**, 266, 1216.

[11] Fenter, P.; Eberhardt, A.; Liang, K. S.; Eisenberger, P. J. Chem. Phys, **1997**, 106, 1600.

[12] Camillone III, N.; Leung, T. Y. B.; Scoles, G. Surface Science, **1997**, 373, 333.

[13] Schwartz, P.; Schreiber, F.; Eisenberger, P.; Scoles, G. Surface Science, **1999**,423, 208.

[14] Camillone III, N.; Chidsey, C. E. D.; Eisenberger , P.; Fenter, P.; Li, J.; Liang, K. S.; Liu, G. Y.; Scoles, G. J. Chem Phys. **1993**, 99, 744.

[15] Poirier, G. E.; Tarlov, M. J. Langmuir, **1994**, 10, 2853.

[16] Delamarche, E.; Michel, B.; Gerber, C.; Anselmatti, D.; Guntherodt, H. J.; Wolf, H.; Ringsdorf, H. Langmuir, **1994**, 10, 2869.

[17] Dishner, M. H.; Hemminger, J. C.; Feher, F. J. Lagmuir, **1997**, 13, 2318.

[18] Voets, J.; Gerritsen, J. W.; Grimberge, R. F. P.; van Kempen, H. Surf. Sci. **1998**, 399, 316.

[19] Yourdshahyan, Y.; Zhang, H. K.; Rappe, A. M. Phys. Rew. B, **2001**, 63, 081405(R).

[20] Gronbeck, H.; Curioni, A.; Andreoni, W. J. Am. Chem. Soc. **2000**, 122, 3839.

[21] Hayashi, T.; Morikawa, Y.; Nozoye, H. J. of Chem. Phys. **2001**, 114, 7615.

[22] Vargas, M. C.; Giannozzi, P.; Selloni, A.; Scoles, G. *J. Phys. Chem. B* **2001,** *105,* 9509.

[23] Nuzzo, R. G.; Zegarski, B. R.; Dubois, L. H. J. Am. Chem. Soc. **1987**, 109, 733.

[24] Ishida, T.; Motamoto, S.; Mizutami, W.; Motomatsu, M.; Tokumato, H.; Hokhari, H.; Azehera, H.; Fujihara, M. Langnuir, **1997**, 13, 3262.

[25] Heister, K.; Allara, D. L.; Bahnck, K.; Frey, S.; Zharnikov, M.; Grunze, M. Langmuir, **1999**, 15, 5440

[26] Noh, J.; Hara, M. Langnuir, **2000**,16 2045

[27] Daniel Farias, Private communication, **2001**.

[28] Camillone, N. Ph. D. thesis, Princeton University, **1994**.

[29] Schwartz, P. Ph. D. thesis, Princeton University, **1998**.

[30] Poelsema B.; Comsa G. Scattering of Thermal Energy Atoms from Disordered Surfaces, Springer-Verlag: Berlin Heidelberg,1989

[31] Camillone III, N.; Eisenberger, P.; Leung, T. Y. B.; Schwartz, P.; Scoles, G.; Poirier, G. E.; Tarlov, M. J. J. Chem. Phys. **1994**, 101, 11031.

[32] Gerlach, R.; Polanki, G.; Rubahn, H. –G. Appl. Phys. A **1997**,65, 375.

[33] Redhead, P. Vacuum, **1965**, 12, 103.

[34] Lavrich, D. J.; Wetterer, S. M.; Bernasek, S. L.; Scoles, G. J. Phys. Chem, **1998**, 102, 3456.

[35] Wetterer, S. M.; Lavrich, D. J.; Cummings, T.; Bernasek, S. L.; Scoles, G. J. Phys. Chem, **1998**, 102, 9267. The errors in this model can be as much as 8.6% for thiol molecules, the error given in the text is calculated by assuming an error of 5%.

[36] Nuzzo, R. G.; Dubois L. H.; Allara D. H. J. Am. Chem. Soc. **1990**, 112, 558.

Figure Captions

Figure 1. a) Schematic representation of diffraction geometry. During measurements incidence angle θ_i is kept constant at 60 ± 0.5^o and detector is rotated in the scattering plane, which is defined by the incident beam, surface normal and detector. Parallel momentum transfer, $\Delta K_{//}$, is equal to $K_f - K_i$. b) Schematic of the inner part of the Helium atom diffraction apparatus (RS: radiation shield, DL: dose line, HB: incident helium beam, XL: crystal, BD: bolometer detector).

Figure 2. a) Evolution of surface structure for various exposure and annealing periods that are detailed in the text. Scans were taken along gold nearest neighbor direction ($\phi=0^o$). Expected diffraction peak positions of $(3x2\sqrt{3})$ super lattice are indicated by lines. b) Specular intensity (■) is multiplied by 10000 and (1,0) (▲) and (2,0) (▼) hexagonal peaks are normalized to specular signal. Width of the (2,0) hexagonal peak (●) is also shown.

Figure 3. a) Diffraction pattern obtained after structure 1 is annealed at 325 K for 15 minutes. b) Diffraction pattern obtained when structure 1 is annealed at 330 K for 40 minutes. When this structure is annealed at 330 K for 60 more minutes c) is obtained.

Figure 4. a) Raw specular reflectivity data as a function of temperature for two different surface structures, structure 3 (——) , structure 1 (— —), and the specular reflectivity of clean Au(111) (———) that is used for sensitivity correction. Differentiation of specular reflectivity before sensitivity correction results in curves, (· · ·) for structure 3

and (— · — ·) for structure 1. b) After correction for Debye-Waller attenuation and bolometer sensitivity, curves (──) and (— —) are obtained for structure 3 and structure 1 respectively. Differentiation of these corrected data results in traditional TPD curves, (· · · ·) for structure 3 and (— · — ·) for structure 1. All the curves except the raw specular reflectivity of structure 1, structure 3 and clean Au(111) are smoothed by adjacent point averaging.

Figure 5. Diffraction scans taken along four different azimuthal angles. $\phi=0^{o}$ corresponds to <1-10> and $\phi=30^{o}$ corresponds to <11-2> direction. Peaks at –1.45, -2.90, -4.36 $Å^{-1}$ along <1-10> and peaks at –2.5, -4.9 $Å^{-1}$ along <11-2> direction correspond to ($\sqrt{3}$ x $\sqrt{3}$)R30^{o} hexagonal lattice. Expected positions of (3x2$\sqrt{3}$) lattice points in <1,-1,0> (<1,-2,0>) direction are indicated by solid lines (dashed lines).

Figure 6. Reciprocal space plot of the experimental peak positions (○). Reciprocal space for (3x2$\sqrt{3}$) super lattice and ($\sqrt{3}$ x $\sqrt{3}$)R30^{o} hexagonal lattice are indicated by (●) and (□) symbols respectively. It should be noted that experimental points (○) are not scaled to intensity. The experimental points which could not be assigned to any (3x2$\sqrt{3}$) lattice point are shown by ⊗. The dashed box represents the resolution function of the apparatus.

Figure 7. a) Real space representation of (3x2$\sqrt{3}$) unit cell. Open circles represent gold atoms and filled circles represent thiolate molecules. The adsorption sites of thiolate

molecules are not to be inferred from this figure. a = 8.68 Å, b = 10.02 Å. b) Reciprocal space representation of (3x2$\sqrt{3}$) structure. The unit cell represented with open circles (○), corresponds to real space lattice shown in a), will be indexed with a single prime (') in the text, open squares and crosses indicate diffraction from the two equivalent types of domains rotated ±120^{o} with respect to first one and will be indexed with double ('') and triple primes (''') respectively in the text. The three patterns coincide at the positions of the simple ($\sqrt{3}$ x $\sqrt{3}$)R30^{o} lattice.

Figure 8. Intensity ratios of the (0,-1)'' peak to (-1,0)' peak and (0,-2)'' peak to (-2,0)' peak of (3x2$\sqrt{3}$)lattice. $I_{(0,-1)''}$ / $I_{(-1,0)'}$ is denoted by filled squares (■), $I_{(0,-2)''}$ / $I_{(-2,0)'}$ is denoted by filled diamonds (◆).

Figure 9. Full coverage (3x2$\sqrt{3}$) unit cell structure proposed by Vargas et al. [21]. Orange, yellow, green and white circles represent gold, sulfur, carbon and hydrogen atoms respectively.

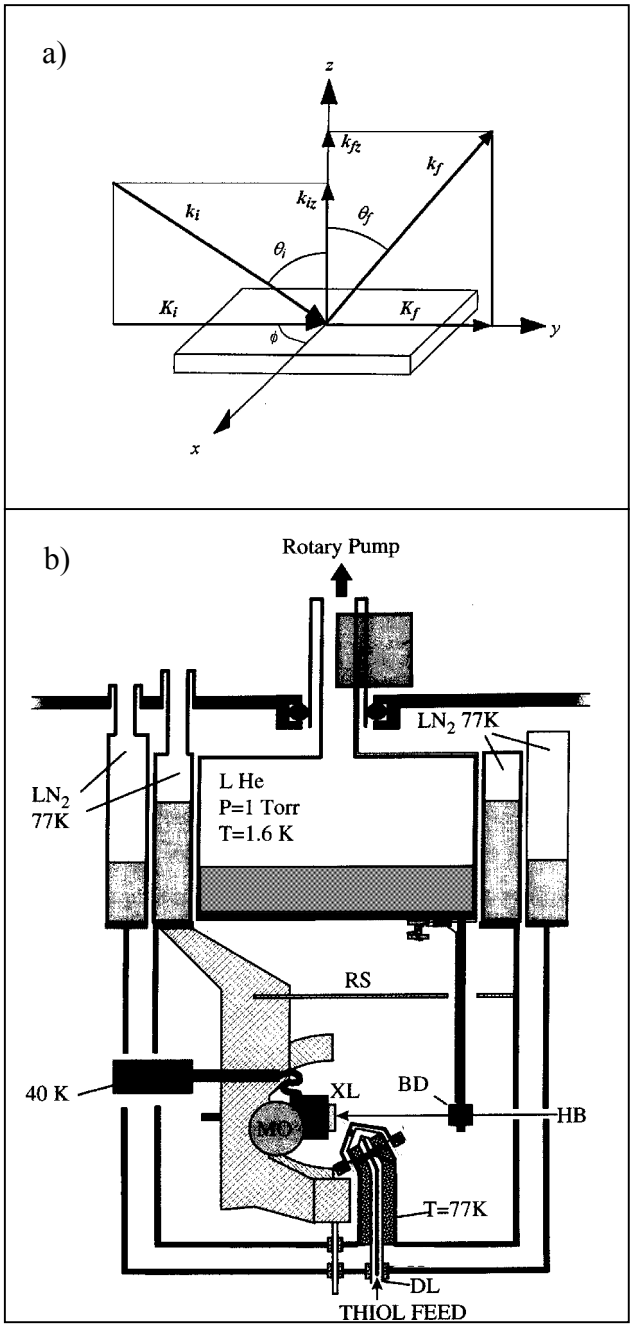
a)
z
k_{fz}
k_f
k_i
k_{iz}
θ_f
θ_i
K_i
K_f
y
ϕ
x
b)
Rotary Pump
LN_2 77K
LN_2
77K
L He
P=1 Torr
T=1.6 K
RS
40 K
XL
BD
HB
MD
T=77K
DL
THIOL FEED

Figure 1

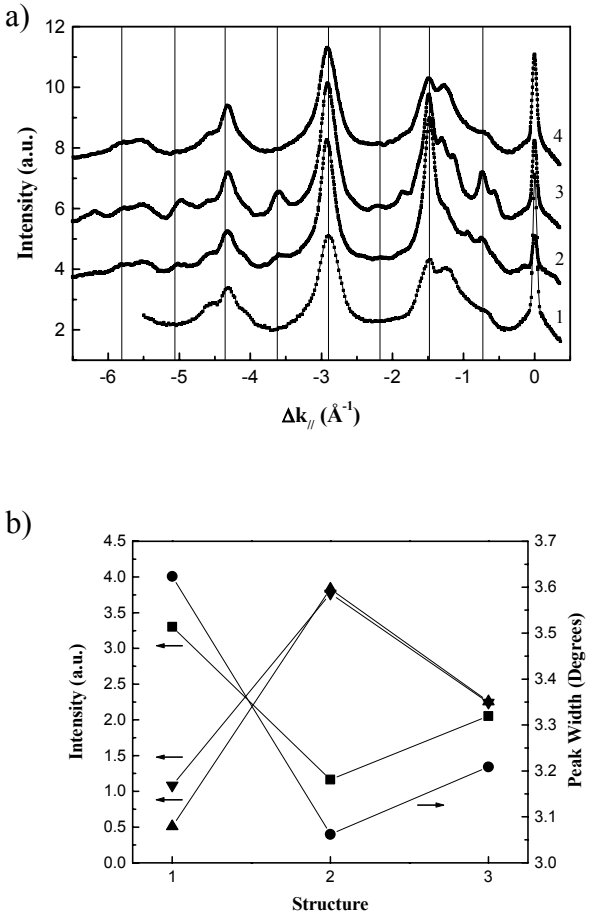
a)
Intensity (a.u.)
$\Delta k_{//}$ (Å^{-1})
1
2
3
4
b)
Intensity (a.u.)
Peak Width (Degrees)
Structure

Figure 2

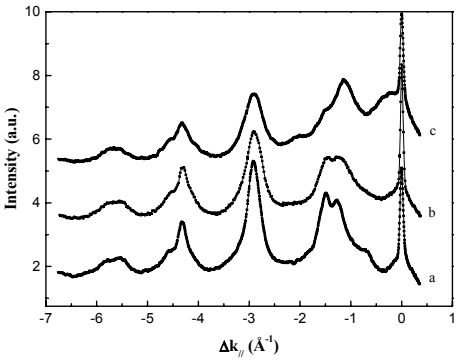

Figure 3

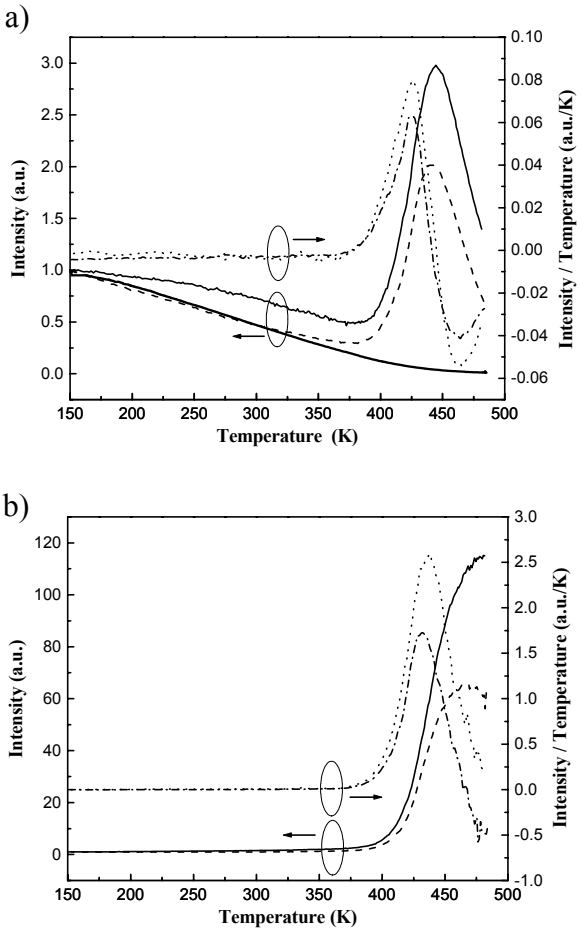
a)
Intensity (a.u.)
Intensity / Temperature (a.u./K)
Temperature (K)
b)
Intensity (a.u.)
Intensity / Temperature (a.u./K)
Temperature (K)

Figure 4

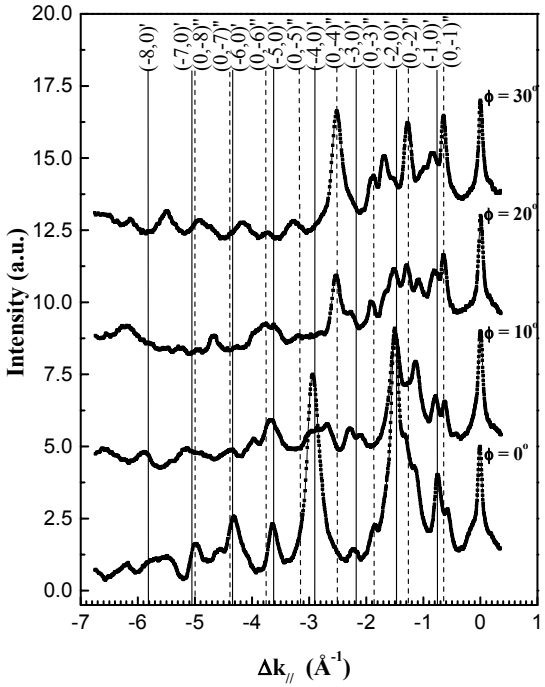
(-8,0)'
(-7,0)'
(0,-8)"
(0,-7)"
(-6,0)'
(0,-6)"
(-5,0)'
(0,-5)"
(-4,0)'
(0,-4)"
(-3,0)'
(0,-3)"
(-2,0)'
(0,-2)"
(-1,0)'
(0,-1)"
ϕ = 30°
ϕ = 20°
ϕ = 10°
ϕ = 0°
Intensity (a.u.)
Δk// (Å-1)

Figure 5

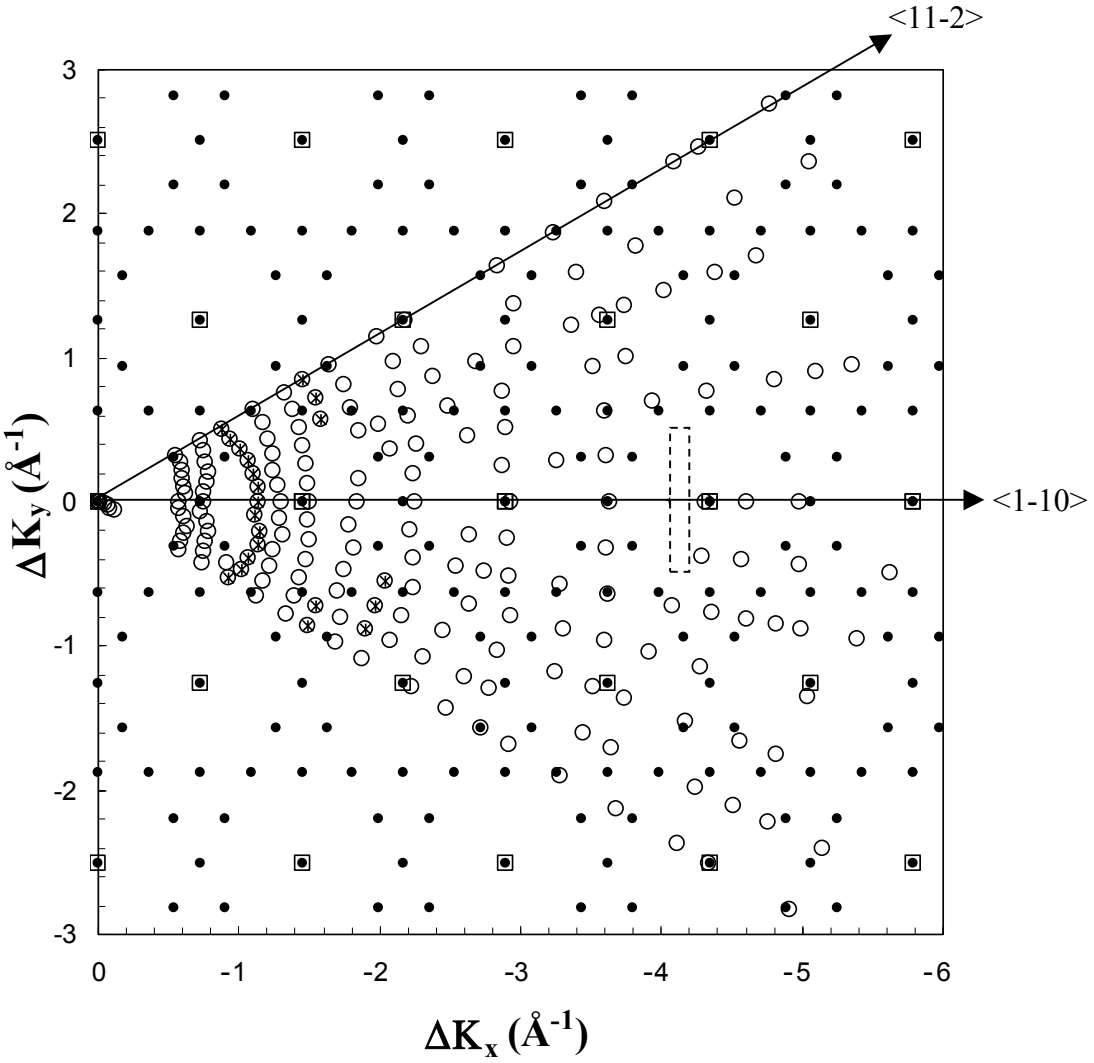

Figure 6

a)

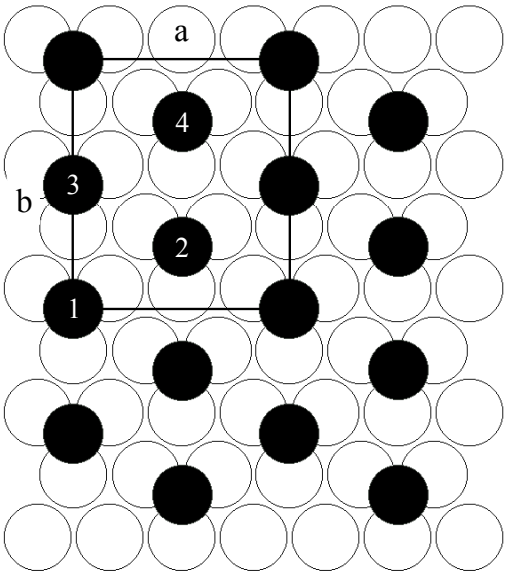

b)

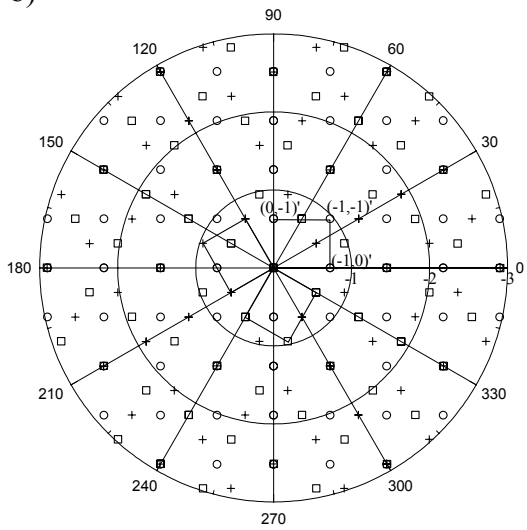

Figure 7

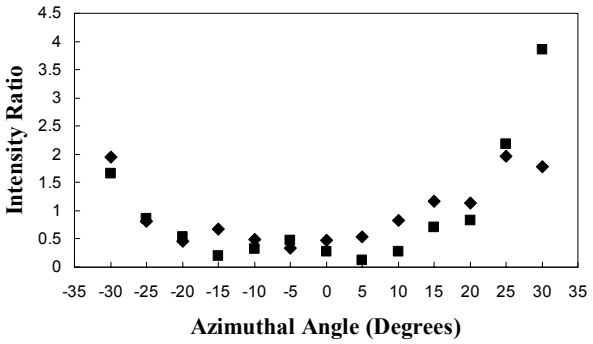
Intensity Ratio
4.5
4
3.5
3
2.5
2
1.5
1
0.5
0
-35 -30 -25 -20 -15 -10 -5 0 5 10 15 20 25 30 35
Azimuthal Angle (Degrees)

Figure 8

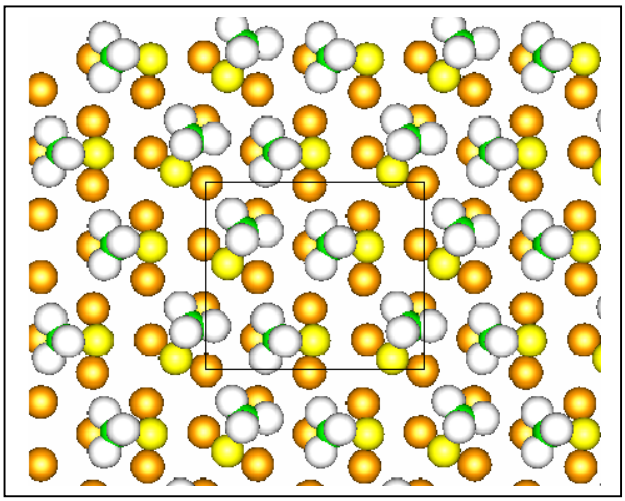

Figure 9